Low-energy collective Gamow-Teller states and isoscalar pairing interaction

C. L. Bai,[1] H. Sagawa,[2,3] G. Colò,[4] Y. Fujita,[5,6] H. Q. Zhang,[7,8] X. Z. Zhang,[7] and F. R. Xu[8]
[1]*School of Physical Science and Technology, Sichuan University, Chengdu 610065, China*
[2]*Center for Mathematics and Physics, University of Aizu, Aizu-Wakamatsu, Fukushima 965-8560, Japan*
[3]*RIKEN, Nishina Center, Wako 351-0198, Japan*
[4]*Dipartimento di Fisica, Università degli Studi di Milano and INFN, Sezione di Milano, 20133 Milano, Italy*
[5]*Research Center for Nuclear Physics, Osaka University, Ibaraki, Osaka 567-0047, Japan*
[6]*Department of Physics, Osaka University, Toyonaka, Osaka 560-0043, Japan*
[7]*China Institute of Atomic Energy, Beijing 102413, China*
[8]*School of Physics and State Key Laboratory of Nuclear Physics and Technology, Peking University, China*
(Received 5 July 2014; revised manuscript received 12 September 2014; published 26 November 2014)

The Gamow-Teller (GT) strength distributions and isobaric analog resonance (IAR) states of several $N = Z + 2$ nuclei with mass number $A = 42$–58 are studied by using a self-consistent Skyrme Hartree-Fock-Bogoliubov method plus quasiparticle random phase approximation (HFB+QRPA) formalism. The isoscalar spin-triplet pairing interaction is included in QRPA on top of the isovector spin-singlet one in the HFB method. It is found that the isoscalar pairing correlations mix largely the $(\nu j_> \rightarrow \pi j_<)$ configurations into the low-energy states, and this mixing plays an important role in the formation and in the collectivity of these low-energy states. Furthermore, the observed excitation energy of the low-energy GT state with respect to the IAR can be well reproduced when the strength of isoscalar pairing is about 1.0–1.05 times that of the isovector pairing, irrespective of the adopted Skyrme interactions. In $N = Z + 2$ nuclei in the middle of the pf-shell, a mutual cooperative effect of isoscalar pairing and tensor interaction is found; namely, the tensor force reduces the spin-orbit splittings and enhances the effect of the isoscalar pairing.

DOI: 10.1103/PhysRevC.90.054335 PACS number(s): 21.30.−x, 21.60.Jz, 24.30.Cz, 25.40.Kv

I. INTRODUCTION

The effective nucleon-nucleon interactions that are employed within self-consistent mean-field approaches have recently reached a high level of sophistication, and have become quite successful in describing many nuclear properties. Though they can be based on different kinds of *Ansätze*, as a rule central, spin-orbit, and tensor terms show up. In open-shell nuclei the pairing interaction or, in fact, its isovector ($T = 1$, $S = 0$) part, was originally introduced to account for the odd-even binding energy staggering and the gap in the excitation spectrum of even-even and odd-A nuclei [1–3]. One of the widely used mean-field approaches is based on zero-range Skyrme forces: in this case, Hartree-Fock (HF) + Bardeen-Cooper-Schrieffer (BCS) equations [4] or Hartree-Fock-Bogoliubov (HFB) equations [5], which include the pairing interaction, are solved to study the ground state properties of the open-shell nuclei [6–9]. On top of this ground-state solutions, the self-consistent quasiparticle random-phase approximation (QRPA) has been adopted by some authors to study the collective excited states [10–15].

The parameters that characterize the effective interactions can be fitted by using empirical properties of uniform nuclear matter as well as a few ground-state (or sometimes excited state) properties. However, some channels of the interactions are not well constrained, one of the clearest examples being the pairing interaction between protons and neutrons in the isoscalar spin-triplet ($T = 0$, $S = 1$) channel. Indeed, there is no consensus on the observables that can be directly related to such a channel, and signatures of strong neutron-proton particle-particle (pp) correlations have not yet been found, despite several efforts [16–22].

It has been well known that one of the effects of this isoscalar spin-triplet force is to give rise to the deuteron bound state. Although some speculations have been made about the relevance of a n-p pairing force in nuclei with $N = Z$, there is no unambiguous evidence of its effects, let alone evidence of a p-n condensate. Effects of isoscalar pairing may be present in charge-exchange excitations and related phenomena. In Refs. [12,23,24] it has been shown that in self-consistent HFB + QRPA calculations, the isoscalar pairing interaction shifts low-energy Gamow-Teller (GT) strength downward so that by fitting the n-p pairing strength, at least locally, one can account for the β-decay half-life in neutron-rich nuclei which are important for the r-process nucleosynthesis. The isoscalar pairing interaction is also important for the double-β decay [25]. In Ref. [26], the $T = 0$ pairing is included in HF-BCS plus QRPA calculations which can well reproduce the energy difference between the Gamow-Teller resonance (GTR) and isobaric analog resonance (IAR) main peaks. However, since not only the isoscalar pairing but other terms of the effective interactions such as the spin two-body terms, spin-orbit one-body term, and tensor terms may also affect the main peak and low-energy tail of GTR [27–31], one could not extract from those calculations firm constraints for the isoscalar pairing interaction. Moreover, the nuclei studied so far have neutron excess and are not close to the regions where isoscalar pairing effects are expected to show up. At the same time, the higher order multipole of charge-exchange transitions, such as the spin-dipole and spin-quadrupole transitions, will receive contributions from both the isoscalar and the isovector pp channels; therefore, one is bound to come back to GT calculations and consider specific

nuclei and/or specific properties to pin down unambiguous information about isoscalar pairing.

In Ref. [32], a two-peaked structure was observed in the $N = Z$ nucleus ^{56}Ni and this can provide some insightful information on the isoscalar pairing. Then, the GT transitions in ^{56}Ni together with other $N = Z$ nuclei were studied by employing the HFB + QRPA theory [33], and this study has highlighted the formation of low-energy GT states in several f-shell nuclei, induced by the isovector and isoscalar pairing interactions and having reasonably strong strength. Recently, it was reported that strong GT states are experimentally observed, only slightly higher than the IAR, in some $N = Z + 2$ nuclei with mass number $A = 42$–54 [34]. Due to the specific selection rules, the GT transitions connect either $j_{\gtrless}(= l \pm 1/2)$ and $j_{\gtrless}(= l \pm 1/2)$ single-particle states, or $j_{\gtrless}$ and $j_{\lessgtr}$ single-particle states, while the IAR is only made up with the former type of transitions. Usually, the former type of transitions is ≈3–7 MeV lower than the latter type of transitions due to the spin-orbit splitting. Therefore, the GT strength is split in two regions: although residual interaction terms move the strength with respect to its location in terms of unperturbed particle-hole (ph) transition, still we can say that roughly the high-energy region is usually about 3–7 MeV higher than the low-energy region. The high-energy region is usually the one in which most of the strength is found in nuclei with neutron excess $N > Z + 2$. Consequently, in these nuclei the main peaks of GT transitions are found at much higher energy than the IAR states except very heavy nuclei such as ^{208}Pb. On the other hand, the lowest GT states observed in Ref. [34] are the low-energy transitions which are expected to be more sensitive to isoscalar pairing because they must involve mainly time-reversed p-n orbits. Moreover, in Ref. [35], Tanimura *et al.* applied a three-body model to study the energy inversion of 1^+ and 0^+ states that determine the character of the ground states of several odd-odd $N = Z$ nuclei in p-, sd-, and pf-shell regions by including the spin-triplet pairing. They have pointed out the important role of strong spin-triplet pairing interaction not only for the energy, but also the GT and magnetic dipole transitions of these nuclei.

In this paper, we apply the HFB + QRPA method to study the GT states excited from some $N = Z + 2$ nuclei with mass number $A = 42$–54 by charge exchange reactions that have been measured by Fujita and collaborators [34]. Our specific purpose in this paper is to find a clear, unambiguous signature of the isoscalar pairing and even a quantitative constraint for its strength. This paper is structured as follows. In Sec. II we briefly describe the HFB + QRPA method used in our calculation. In Sec. III we show the evolution of the GT strength distributions as a function of mass number and isoscalar pairing strength, focusing on the emergence of low-lying GT states. In Sec. IV we discuss each nucleus in more detail, by focusing on the mechanism through which the isoscalar pairing strength creates low-lying GT states, and disentangling the effect of tensor correlations.

II. FORMALISM

As explained in the Introduction, we aim to pin down constraints on the different channels of the pairing interaction. We introduce them in the form of density-dependent, contact (i.e., zero-range) surface pairing interactions,

$$V_{T=1}(\mathbf{r_1},\mathbf{r_2}) = V_0 \frac{1-P_\sigma}{2}\left(1-\frac{\rho(\mathbf{r})}{\rho_o}\right)\delta(\mathbf{r_1}-\mathbf{r_2}), \quad (1)$$

$$V_{T=0}(\mathbf{r_1},\mathbf{r_2}) = f V_0 \frac{1+P_\sigma}{2}\left(1-\frac{\rho(\mathbf{r})}{\rho_o}\right)\delta(\mathbf{r_1}-\mathbf{r_2}), \quad (2)$$

where $\mathbf{r} = (\mathbf{r_1} - \mathbf{r_2})/2$, ρ_0 is taken to be $\rho_0 = 0.16$ fm^{-3}, and P_σ is the spin exchange operator. Since the $T = 0$ pairing strength is not yet well constrained, we take f as a free parameter; in our QRPA calculations, it takes the values 0.0, 0.5 0.9, 0.95, 1.0, 1.05, and 1.1.

In the mean-field channel, we employ in our calculations the Skyrme parameter sets SGII [27], SGII + Te3 [36], and SAMi [37]. We remind that SGII was fitted to reproduce proper values of the Landau parameter G_0'. In the case of SAMi the same strategy was adopted on top of the Lyon force fitting protocol, and moreover we checked that one can well reproduce the GT excitation energy of some closed-shell nuclei. Finally the SGII + Te3 interaction reproduces the GT and spin-dipole excitation energies in ^{90}Zr and ^{208}Pb with the inclusion of the tensor force.

In HFB the maximum angular momentum $J_{\max} = 15/2$, and the maximum quasiparticle energy cutoff 180 MeV, are used. The strength of the $T = 1$ pairing is determined to reproduce the odd-even mass staggering gap $\Delta_n^{(4)} = [B(N-2,Z) - 3B(N-1,Z) + 3B(N,Z) - B(N+1,Z)]/4$ in these f-shell nuclei, and results are $V_0 = -446.2$, -430.6, and -460.7 MeV fm^3 for SGII, SGII + Te3, and SAMi, respectively. The mean pairing gaps of these five nuclei are shown in Fig. 1. We stress again that the results labeled by SGII + Te3 are calculated with tensor force, and those labeled by SAMi and SGII are calculated without tensor force. For SGII + Te3 and SAMi, the $T = 1$ pairing strengths are adjusted to reproduce the value of $\Delta_n^{(4)}$ within 0.2 MeV difference, while SGII cannot attain this criterion.

After HFB calculations, in order to obtain the canonical basis, we diagonalize the density matrix by using an intermediate basis, that is, by orthonormalizing the set of functions

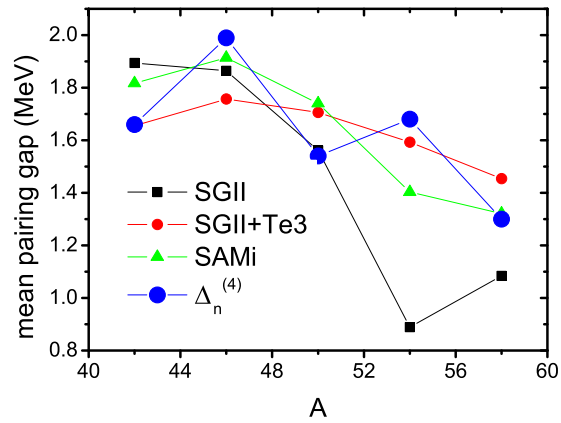

FIG. 1. (Color online) Mean neutron pairing gaps in ^{42}Ca, ^{46}Ti, ^{50}Cr, ^{54}Fe, and ^{58}Ni compared with the quantity $\Delta^{(4)}$ described in the text.

$\{\phi_1^k + \phi_2^k\}$ for each $(l,\ j,\ q)$, q being a label for protons or neutrons and ϕ_1^k and ϕ_2^k being the upper and lower components of the quasiparticle state k [11]. After the canonical basis is obtained, we solve the the pn-QRPA equation

$$\begin{pmatrix} A & B \\ -B & -A \end{pmatrix} \begin{pmatrix} X \\ Y \end{pmatrix} = E_{\mathrm{QRPA}} \begin{pmatrix} X \\ Y \end{pmatrix}, \tag{3}$$

in which

$$\begin{aligned} A_{pn,p'n'} &= E_{pp'}\delta_{nn'} + E_{nn'}\delta_{pp'} \\ &\quad + V^{\mathrm{ph}}_{pn,p'n'}(u_p v_n u_{p'} v_{n'} + v_p u_n v_{p'} u_{n'}) \\ &\quad + V^{\mathrm{pp}}_{pn,p'n'}(u_p u_n u_{p'} u_{n'} + v_p v_n v_{p'} v_{n'}), \end{aligned} \tag{4}$$

$$\begin{aligned} B_{pn,p'n'} &= V^{\mathrm{ph}}_{pn,p'n'}(v_p u_n u_{p'} v_{n'} + u_p v_n v_{p'} u_{n'}) \\ &\quad - V^{\mathrm{pp}}_{pn,p'n'}(u_p u_n v_{p'} v_{n'} + v_p v_n u_{p'} u_{n'}). \end{aligned} \tag{5}$$

The effective residual ph interaction is in principle composed of terms derived from the Skyrme, Coulomb, and pairing interactions. These terms are derived by the second derivative of the energy density functional with respect to the density [11,38]. Due to the isospin selection rules, the contribution of the Coulomb interaction to the pn-QRPA matrix element is zero. In addition, the pairing interactions adopted in the present study do not provide any contribution to the ph channel because of their linear dependence on the density. In the pp channel, there are contributions from $T = 1$ and $T = 0$ pairing interactions defined in Eqs. (1) and (2). For the IAR, only $T = 1$ pairing gives a finite contribution, while this statement is true for the $T = 0$ pairing in the case of the GTR. This is a property of zero-range pairing forces.

After diagonalizing the QRPA matrix, the strength associated with the operator $\hat{O}$ can be calculated by

$$B^{\nu}_{-} = \left| \sum_{pn} \left(X^{\nu}_{pn} u_p v_n + Y^{\nu}_{pn} \tau v_p u_n \right) \langle p || \hat{O}_{-} || n \rangle \right|^2, \tag{6}$$

$$B^{\nu}_{+} = \left| \sum_{pn} \left(X^{\nu}_{pn} \tau v_p u_n + Y^{\nu}_{pn} u_p v_n \right) \langle p || \hat{O}_{+} || n \rangle \right|^2, \tag{7}$$

with τ being ± 1 according to whether the operator $\hat{O}$ is even or odd under time reversal. We can also define the transition amplitude (A_{pn}) of a configuration such as that in the t_- channel,

$$A_{pn} = \left(X^{\nu}_{pn} u_p v_n + Y^{\nu}_{pn} \tau v_p u_n \right) \langle p || \hat{O}_{-} || n \rangle. \tag{8}$$

This can be used to evaluate the contribution of a p-n configuration to a given collective excited state.

For GT and IAR, the operator $\hat{O}_{\pm}$ reads

$$\hat{O}_{\mathrm{GT}\pm} = \sum_{im} t^i_{\pm} \sigma^i_m, \tag{9}$$

$$\hat{O}_{\mathrm{IAS}\pm} = \sum_{im} t^i_{\pm}, \tag{10}$$

respectively, in terms of the standard isospin operators, $t_{\pm} = \frac{1}{2}(t_x \pm i t_y)$. We finally remind that, in the QRPA calculations, there exists a model-independent non-energy-weighted sum rule (NEWSR) for the GT and IAR transitions:

$$S_{\mathrm{GT}-} - S_{\mathrm{GT}+} = 3(N - Z), \tag{11}$$

$$S_{\mathrm{IAR}-} - S_{\mathrm{IAR}+} = N - Z. \tag{12}$$

In our QRPA calculations the GT sum rule of each nucleus is checked and found to fulfill the model-independent channel within 1%.

III. LOW ENERGY COLLECTIVE GT STATE IN N = Z + 2 NUCLEI WITH A = 42–58

The GT strength distributions calculated with the factor f taking the values $f = 0.0$, 0.5, 1.0, and 1.1, together with the IAR states, in ^{42}Ca, ^{46}Ti, ^{50}Cr, ^{54}Fe, and ^{58}Ni are shown in Fig. 2, where the excitation energy E_x is shown from the ground state of the initial nuclei. The Skyrme parameter set SAMi is used. This force has been fitted so as to reproduce the GT main peak energies in stable nuclei ^{90}Zr and ^{208}Pb.

As shown in the figure, when $f = 0.0$,0.5, which means without or with a weak isoscalar pairing, the GT strengths are found in the high-energy region, defined here as the region above 14 MeV and thus, also above the IAR. More precisely, in ^{42}Ca and ^{46}Ti, the GT peaks are split into two peaks, while a single peak is found in ^{50}Cr, ^{54}Fe, and ^{58}Ni. The low-energy peak is located above the IAR in each nucleus. The strength of the low-energy peak is decreasing for the larger mass nuclei and is almost invisible in ^{58}Ni. The main peak is found at about 16–17 MeV in each nucleus, which is about 5 to 6 MeV higher than the low-energy peak, and about 7–8 MeV higher than the IAR peaks.

When the factor f is increased up to values 1.0–1.1, the low-energy peaks are shifted downward close to the IAR, and even below the IAR if $f = 1.1$. Moreover, the strength in the low-energy peaks are dramatically enhanced, especially in ^{42}Ca and ^{46}Ti, exhausting about 70% of the Gamow-Teller sum rule $3(N - Z) = 6$. In ^{50}Cr the low-energy peaks exhausts a similar amount of GT strength as the high-energy peak. In ^{54}Fe and ^{58}Ni, the strength in the low-energy peaks is also increased but still not strong compared with the high-energy peak.

Thus, it is quite clear that the isoscalar pairing is the driving force to create some collective low-energy GT states in these $N = Z + 2$ nuclei. More quantitative aspects about the strength of those states, and details about the underlying mechanism will be discussed in the next section.

The strength evolution in the low energy peak can be qualitatively understood by the coefficients of the pp and ph terms of Eq. (5). In general, the ph residual interaction in the spin-isospin channel is repulsive and shifts the strength upward (especially in the high-energy peak which is dominated by the $j_> \rightarrow j_<$ transition); the pp residual interaction is attractive and shifts the low- and high-energy peaks downward. In the cases under study, the important configurations are $(\nu 1f_{7/2}, \pi 1f_7/2)$ and $(\nu 1f_{7/2}, \pi 1f_{5/2})$, which can be denoted by $j_> \rightarrow j_>$ and $j_> \rightarrow j_<$, respectively. The associated coefficients for the diagonal matrix elements, cfph $\equiv u_p v_n u_p v_n + v_p u_n v_p u_n$ and cfpp $= u_p u_n u_p u_n + v_p v_n v_p v_n$ for the two configurations are displayed in Table. I. One can see that these coefficients change drastically from ^{42}Ca to ^{54}Fe. For the

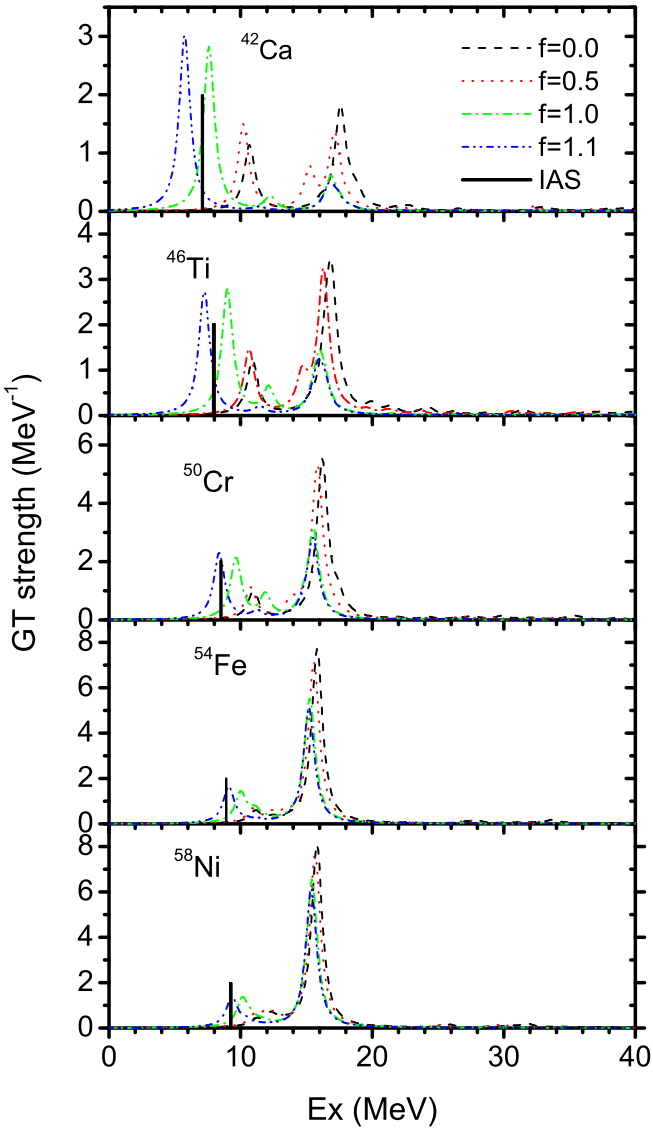

FIG. 2. (Color online) GT strength distributions in ^{42}Ca, ^{46}Ti, ^{50}Cr, ^{54}Fe, and ^{58}Ni obtained by HFB + QRPA calculations with the Skyrme interaction SAMi. The $T = 0$ pairing interaction is included in QRPA by changing the coupling constant f that takes the values $f = 0.0$, 0.5, 1.0, and 1.1 [cf. Eq. (2)]. The vertical black line corresponds to the IAR state. The excitation energy is calculated with respect to the ground state of target nuclei. See the text for a more detailed discussion.

configuration $(\nu 1f_{7/2}, \pi 1f_{5/2})$ in ^{42}Ca, cfpp is four times larger than cfph. This means that in this nucleus the high-energy peak will receive a strong effect from the pp channel, and as a consequence the strength in the high-energy region is shifted largely to the low-energy region. As a result, about 80% of the strength is found in the low-energy region. In ^{46}Ti, the ratio cfpp/cfph decreases to about 1.5 and the QRPA results show again that a substantial portion of the strength is shifted to the low-energy region. In ^{50}Cr, this ratio decreases further to about 0.5. That means that the high-energy region is subject to the effect of the ph interaction, and only a small part of the strength is shifted to the low-energy region. In ^{54}Fe, the ratio becomes about 0.25, so that the effect of pp interaction is marginal, and a very small amount of strength is shifted from the high-energy region to the low-energy region. In ^{42}Ca, it turns out that the ph interaction is very much suppressed and most of the strength is distributed in the low-energy region. In conclusion, our results allow us to clearly pinpoint the competition of ph and pp interactions, and consequently assess the role of the $T = 0$ pairing, even if effects that may change the detail of the strength distribution, such as deformation effects or coupling with complex configurations beyond two-quasiparticle ones, are not included.

IV. SUM RULE VALUES AND MECHANISMS FOR THE EMERGENCE OF LOW-LYING GT STATES

In this section, we discuss the cumulative sum rule and the role of $T = 0$ pairing correlations to enhance the low-energy GT states in each nucleus. We also single out other effects, like that of tensor correlations.

A. ^{42}Ca

Since the tensor correlations have been reported to affect significantly the collective GT and spin-dipole states, we have done calculations using either SGII or SGII + Te3, as explained above.

In Fig. 3, it is shown that the inclusion of tensor force shifts the high-energy peaks downward by about 1.2 MeV in the cases of $f = 0.0$ and 0.5. Although in the case of stronger isoscalar pairing strength the main effect on the high-energy peak is to reduce its strength, we also notice that it is shifted downward by about 1 MeV. On the other hand, the low-energy peaks that appear in the strong $T = 0$ pairing case do not get any significant effect by the tensor correlations, and their peak energies are almost the same when we use either SGII or

TABLE I. Coefficients of the pp and ph terms in Eq. (5), in the case of the diagonal matrix elements associated with the $(\nu 1f_{7/2}, \pi 1f_{7/2})$ and $(\nu 1f_{7/2}, \pi 1f_{5/2})$. The coefficients cfph and cfpp are defined in the text.

	$v^2_{\nu f_{7/2}}$	$v^2_{\pi f_{7/2}}$	$v^2_{\pi f_{5/2}}$	$(\nu 1f_{7/2}, \pi 1f_{7/2})$		$(\nu 1f_{7/2}, \pi 1f_{5/2})$	
				cfpp	cfph	cfpp	cfph
^{42}Ca	0.20	0.00	0.00	0.80	0.20	0.80	0.20
^{46}Ti	0.40	0.21	0.02	0.56	0.44	0.60	0.40
^{50}Cr	0.62	0.43	0.03	0.48	0.52	0.39	0.61
^{54}Fe	0.84	0.66	0.04	0.61	0.39	0.19	0.81

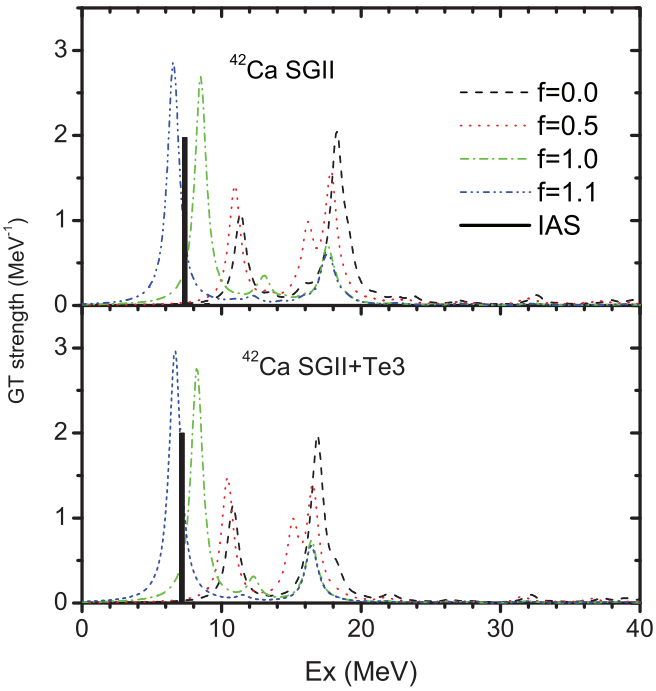

FIG. 3. (Color online) GT strength distributions in ^{42}Ca obtained by HFB + QRPA calculations with the Skyrme interactions SGII and SGII + Te3. The $T = 0$ pairing interaction is included in QRPA by changing the coupling constant f of Eq. (2), that takes the values $f = 0.0$, 0.5, 1.0. The vertical black line corresponds the IAR. The excitation energy is calculated with respect to the ground state of the target nuclei. See the text for a more detailed discussion.

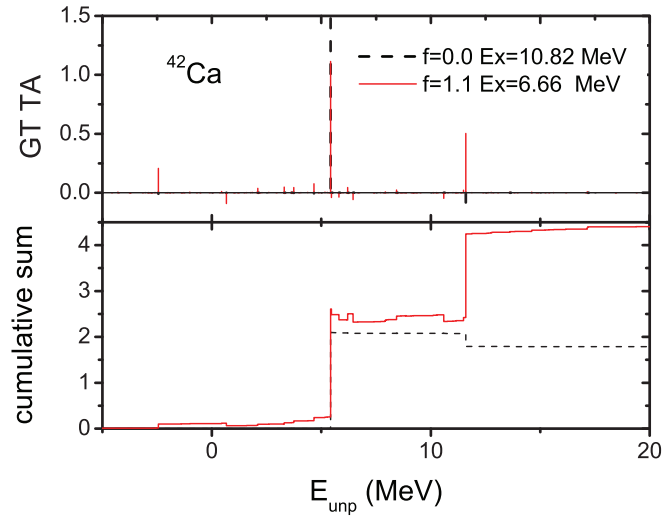

FIG. 4. (Color online) The transition amplitudes (GT TA) (upper panel) defined in Eq. (8) and their cumulative sum defined in Eq. (13) (lower panel) for the low-energy GT state in ^{42}Ca, calculated by using SGII + Te3 with $f = 0.0$ and 1.1.

SGII + Te3. These results indicate that the effect of the tensor force is suppressed on the low-energy peak or overwhelmed by the effect of pairing.

Let us now discuss the mechanism for the enhancement of the GT strength in the low-energy region. In the single-particle picture, the $(j_> \rightarrow j_>)$ transition will be the dominant transition mode in the low-energy region, and this will be $(\pi f_{7/2}, \nu f_{7/2})$ in these $N = Z + 2$ nuclei with $A = 42$–54. On the other hand, the $(j_> \rightarrow j_<)$ transition will contribute as the dominant configuration for the high-energy GT state. We define a quantity that allows us to quantify the contribution of different unperturbed transitions, lying at different excitation energies, namely the cumulative sum of the GT transition matrix elements of Eq. (8) that is defined by the following formula:

$$CS(E_{\rm unp}) = \left| \sum_{pn}^{E_{pn} \leqslant E_{\rm unp}} A(E_{pn}) \right|^2 . \qquad (13)$$

Here the energy $E_{\rm unp}$ corresponds to the difference between proton and neutron "single-particle-like" energies, that are defined as the diagonal matrix elements of the Hartree-Fock field (in the canonical basis). Figure 4 shows the GT transition amplitudes A (upper panel) defined in Eq. (8) and the cumulative sum of these transition amplitudes defined by Eq. (13) for the low-energy GT states as a function of $E_{\rm unp}$ in ^{42}Ca. These low-energy GT states are selected at $E = 10.82$ MeV when $f = 0.0$ and at $E = 6.66$ MeV when $f = 1.1$ (they are calculated by using SGII + Te3, so they are visible in Fig. 3). When there is no isoscalar pairing in QRPA ($f = 0.0$), there is only one dominant configuration $(\pi f_{7/2}, \nu f_{7/2})$ at $E_{\rm unp} = 5.45$ MeV contributing to the GT strength. On the other hand, when a strong isoscalar pairing strength ($f = 1.1$) is taken, that configuration makes still an important contribution, but the configurations $(\pi f_{5/2}, \nu f_{7/2})$ and $(\pi f_{7/2}, \nu f_{5/2})$, respectively at $E_{\rm unp} = 11.6$ and -3.4 MeV, also contribute with the same phase. Altogether, the strong isoscalar pairing increases the GT strength of the state at $E = 6.66$ MeV by more than a factor of 2. This strong collective GT state was called the low-energy super-GT state in Ref. [34], reflecting the fact that the strong transition will be induced between the members of SU(4) "supermultiplet" symmetry.

The cumulative sum of the GT strength is defined as

$$m_0(E) = \sum_n^{E_n \leqslant E} B_{\rm GT-}(E_n) + \int^E \frac{dB_{\rm GT-}(E)}{dE} dE, \qquad (14)$$

taking into account the discrete states at the excitation energy E_n together with the continuum GT strengths. The cumulative sum of the GT strength in ^{42}Ca calculated by the SGII + Te3 interaction with the IS pairing strengths $f = 0.0$, 0.5, 1.05 are shown in Fig. 5. The calculated results are compared with the experimental data taken from Ref. [34]. For ^{42}Ca, the experimental data show that most of the GT strength is concentrated in the lowest GT state at 0.611 MeV, with a small amount of strength distributed around 4 and 10 MeV. The QRPA results with $f = 1.05$ also show most of the strength concentrated in the lowest GT state around 0.6 MeV, with small amounts distributed around 5.5 and 10 MeV. Thus, the calculated results with the strong $T = 0$ pairing show a good agreement with the cumulative sum that has been experimentally measured, while this cumulative sum rule

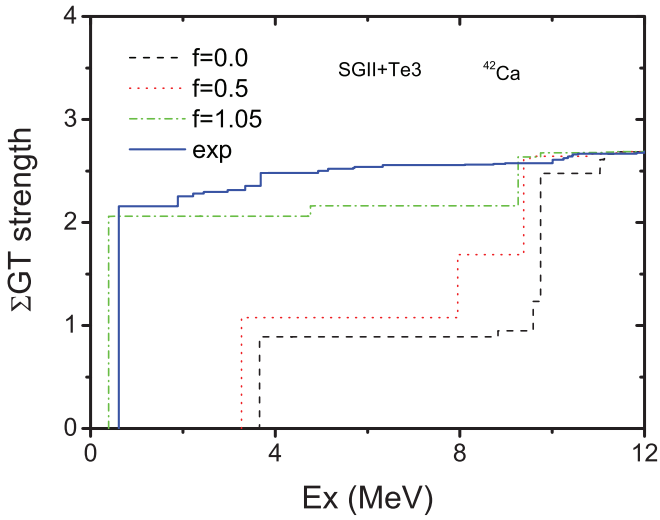

FIG. 5. (Color online) The cumulative sum of the GT strength in ^{42}Ca, calculated by SGII + Te3 interaction with $f = 0.0$, 0.5, 1.05. The blue line is the experimental result taken from Refs. [34]. The excitation energy is referred to the IAR. The maximum values of theoretical GT strengths are normalized to that of the experimental result.

would be very different without $T = 0$ pairing, as in that case there would be not much strength below 3 MeV and there would be no good correspondence with the experimental data.

B. ^{46}Ti

In Fig. 6, the effects of the tensor correlations on the GT states in ^{46}Ti are shown by using SGII and SGII + Te3 interactions. In the case of no or weak $T = 0$ pairing with $f = 0.0$ and 0.5, the high-energy peak is shifted downward

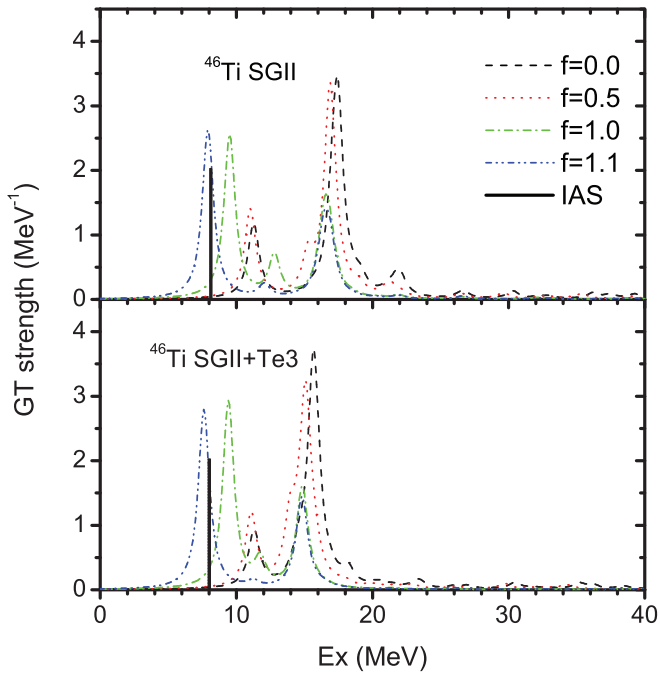

FIG. 6. (Color online) The same as Fig. 3, in the case of ^{46}Ti.

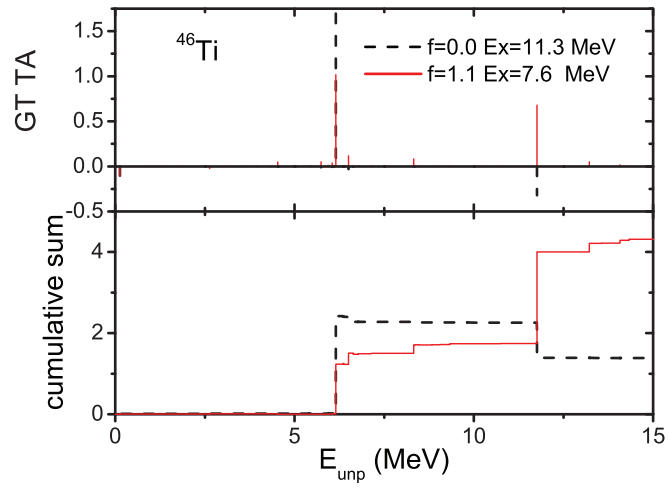

FIG. 7. (Color online) The same as Fig. 4, in the case of ^{46}Ti.

by 1.7 MeV due to the tensor correlations. In the cases of stronger $T = 0$ pairing, the downward shift is quantitatively similar. Since ^{46}Ti has more valence particles in the pf-shell than ^{42}Ca, this energy shift is larger in ^{46}Ti than in ^{42}Ca. For the low-energy peak one obtains again a small effect from the tensor correlations, as in ^{42}Ca. The GT transition amplitudes of the two GT states at 11.3 MeV in the case of $f = 0.0$ and at 7.6 MeV in the case of $f = 1.1$ are shown in Fig. 7. When there is no isoscalar pairing ($f = 0.0$), the configuration $(\pi f_{7/2}, \nu f_{7/2})$ at $E_{\rm unp} = 6.1$ MeV is the dominant configuration while the contribution from the $(\pi f_{7/2}, \nu f_{5/2})$ configuration at $E_{\rm unp} = 11.8$ MeV is smaller and even in opposition of phase. When the strong isoscalar pairing is introduced with $f = 1.1$, the transition amplitude of $(\pi f_{7/2}, \nu f_{7/2})$ decreases, but that of $(\pi f_{7/2}, \nu f_{5/2})$ increases and becomes coherent with the other contribution. Moreover, other small yet non-negligible coherent contributions show up, and this produces a strong GT transition strength as is seen in the lower panel.

The cumulative B(GT) sum for ^{46}Ti is shown in Fig. 8. For ^{46}Ti, the experimental data show that the strength in the

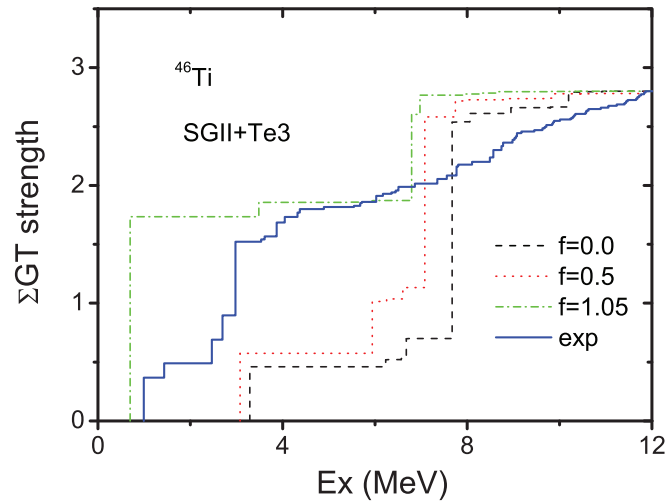

FIG. 8. (Color online) The same as Fig. 5, in the case of ^{46}Ti.

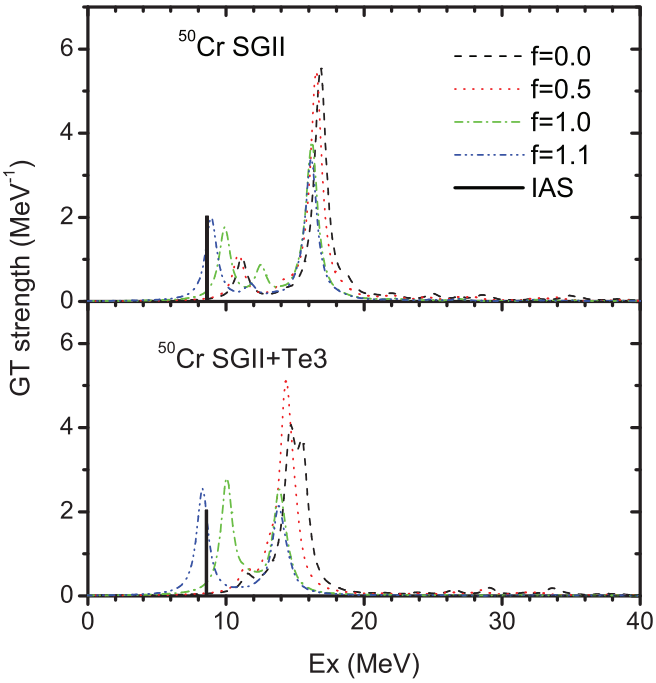

FIG. 9. (Color online) The same as Fig. 3, in the case of ^{50}Cr.

energy region lower than 4 MeV (which is more than half of the total strength) is fragmented into several states, with a lowest strong state at 0.994 MeV, and a bump-like distribution in the 6–11 MeV region. The QRPA results show a concentration of the GT strength around 1 MeV, as well as around 8 MeV, in reasonable agreement with the data.

C. ^{50}Cr

Figure 9 shows the calculated results in ^{50}Cr obtained by using SGII and SGII + Te3, that is, without and with the tensor force respectively. Compared with the two nuclei ^{42}Ca and ^{46}Ti, tensor correlations have larger effects on both the excitation energy and the GT strength; the high-energy peak is shifted downward by about 2 MeV and even the low-energy peak is shifted by about 0.5 MeV. The GT strength of the low-energy peak in the case of strong $T = 0$ pairing with $f \approx 1.0$ is also enhanced by 50% by the tensor correlations. This is due to the fact that ^{50}Cr is a midshell nucleus and gets easily a strong effect from the tensor force.

The transition amplitudes and their cumulative sum are shown in Fig. 10, for the two GT states lying at 11.5 MeV in the case of $f = 0.0$, and at 8.3 MeV in the case of $f = 1.1$, respectively. In the case of no isoscalar pairing, the transition amplitudes show similar features in the case of ^{46}Ti; namely, the contribution of $(\pi f_{7/2}, \nu f_{7/2})$ at $E_{\rm unp} = 6.7$ MeV is the dominant one while $(\pi f_{7/2}, \nu f_{5/2})$ at $E_{\rm unp} = 11.0$ MeV gives a small contribution with the opposite sign. In the case of strong isoscalar pairing, these two configurations display large contributions with the same phase, which enhances the GT strength by about a factor of 8 compared with the state at 11.5 MeV that exists in the case of no isoscalar pairing.

In general, in the three nuclei ^{42}Ca, ^{46}Ti, and ^{50}Cr, the low excitation energy GT state takes a contribution from the

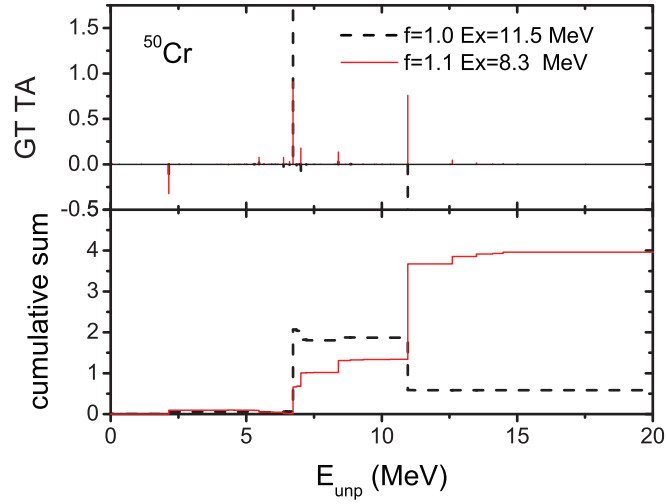

FIG. 10. (Color online) The same as Fig. 4, in the case of ^{50}Cr.

$\nu j_> \to \pi j_>$ state only, in the case of no or weak isoscalar pairing correlations. On the other hand, the isoscalar pairing correlations shift the contribution of the $\nu j_> \to \pi j_<$ amplitude to the low-energy GT state(s) and affect as well the relative phase, so that the *coherent* sum of $\nu j_> \to \pi j_>$ and $\nu j_> \to \pi j_<$ transition amplitudes contributes to build up a relatively strong GT state.

The cumulative B(GT) sum for ^{50}Cr is shown in Fig. 11 for SGII + Te3 with the isoscalar pairing given by $f = 0.0$, 0.5, and 1.05. In ^{50}Cr, the QRPA result with $f = 1.05$ reproduces well the GT strength distribution in the energy region lower than ≈ 6 MeV, while there is only small strength below 5 MeV in the cases of no IS pairing and weak IS pairing with $f = 0.0$ and 0.5, respectively. The calculations show a concentration of the strength in the high-energy region rather than fragmented in a bump-like distribution as observed in the experiment. In general, QRPA does not by construction include all spreading effects and we do not aim at comparing the line shape with experiment in this work.

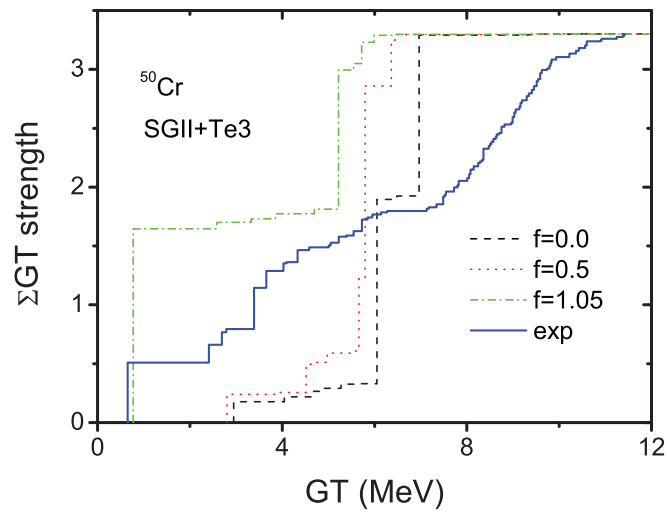

FIG. 11. (Color online) The same as Fig. 5, in the case of ^{50}Cr

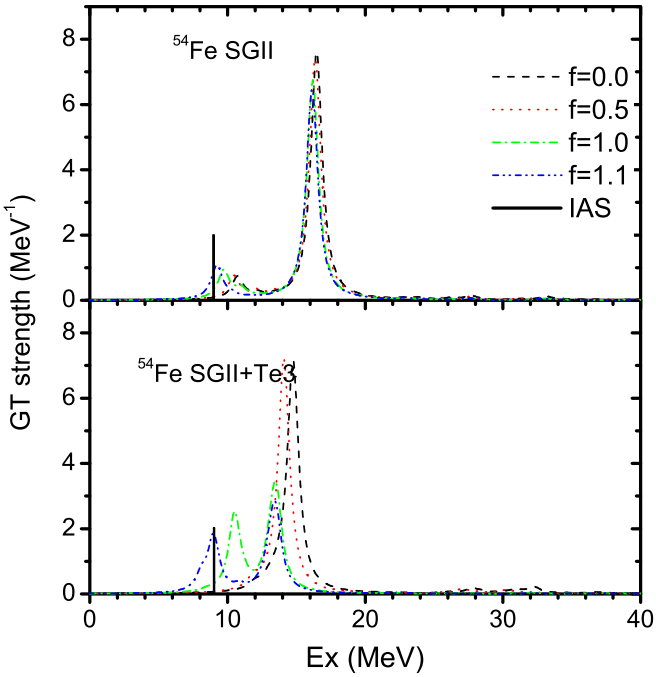

FIG. 12. (Color online) The same as Fig. 3, in the case of ^{54}Fe .

D. ^{54}Fe

The effect of the tensor force is displayed in Fig. 12 by means of the comparison, as above, between the SGII and SGII + Te3 interactions. Compared with the three lighter nuclei with $N = Z + 2$ that we have discussed so far, the tensor correlations in ^{54}Fe are crucial to allow the isoscalar pairing giving an effect. In the upper panel of Fig. 12, one can note that the isoscalar pairing does not change the GT strength distributions, even when it is strong ($f = 1.0$ and 1.1), without the tensor correlations. On the other hand, when tensor correlations are present, the GT strength distribution is markedly affected both in energy and strength by the isoscalar paring, as can be seen in the lower panel of Fig. 12. With the strong isoscalar pairing, the high-energy peak is quenched substantially and shifted downward by more than 2 MeV. At the same time, the low-energy peak is enhanced by a factor of 2 in the case of $f \geqslant 1.0$.

For ^{54}Fe and ^{58}Ni (to be discussed below) the p orbits are also equally important for the GT as the f-shell configurations. In Fig. 13 two states are shown at 12.1 MeV with $f = 0.0$ and 8.9 MeV with $f = 1.1$, respectively. When no isoscalar pairing is introduced with $f = 0.0$, $(\pi p_{3/2}, \nu p_{3/2})$ at $E_{\rm unp} =$ 7.5 MeV is the dominant configuration, while in the case $f =$ 1.1 the two configurations $(\pi f_{7/2}, \nu f_{5/2})$ at $E_{\rm unp} = 10.6$ MeV and $(\pi f_{7/2}, \nu f_{7/2})$ at $E_{\rm unp} = 7.3$ MeV contribute mainly to build a strong GT transition with the same phase. Thus, the cumulative sum is large in the case of strong isoscalar pairing, and the GT strength becomes one order of magnitude stronger than in the $f = 0.0$ case.

The cumulative B(GT) sum for ^{54}Fe is shown in Fig. 14. For ^{54}Fe, there is just about 10% of the total strength distributed in the energy region lower than 4 MeV (with a lowest state at 0.936 MeV) and there is a bump-like strength in the energy

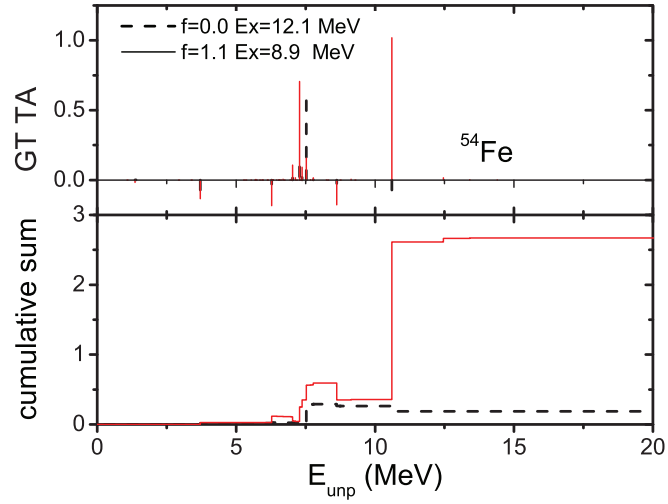

FIG. 13. (Color online) The same as Fig. 4, in the case of ^{54}Fe.

region from 4 to 12 MeV. The QRPA results by SGII + Te3 with the strong isoscalar pairing produce a larger portion of the GT strength in the low-energy region, while with weak or no isoscalar pairing there is essentially no strength below 5 MeV. The QRPA results calculated by SAMi and SGII show about 10% of the strength distributed in the low-energy region with a stronger concentration in the high-energy region at about 7 MeV. Consequently, the QRPA calculations using SAMi in Fig. 2 and SGII in Fig. 12 can reproduce well the portion of the GT strength in the energy region below 4 MeV as compared with SGII + Te3, in which the attractive tensor force tends to shift too much GT strength to the low-energy region.

E. ^{58}Ni

The effect of the tensor force is shown in Fig. 15 by means of a comparison between SGII and SGII + Te3. Just like in the case of ^{54}Fe, the isoscalar pairing does not affect the main GT peak at $E \approx 17$ MeV without the tensor force, while the

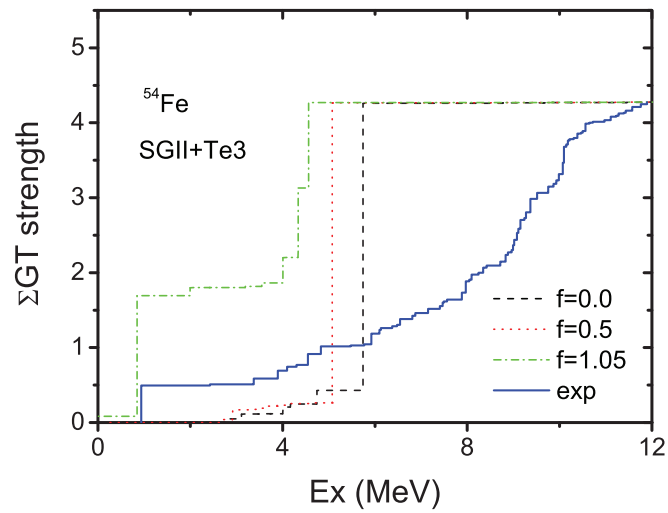

FIG. 14. (Color online) The same as Fig. 5, in the case of ^{54}Fe.

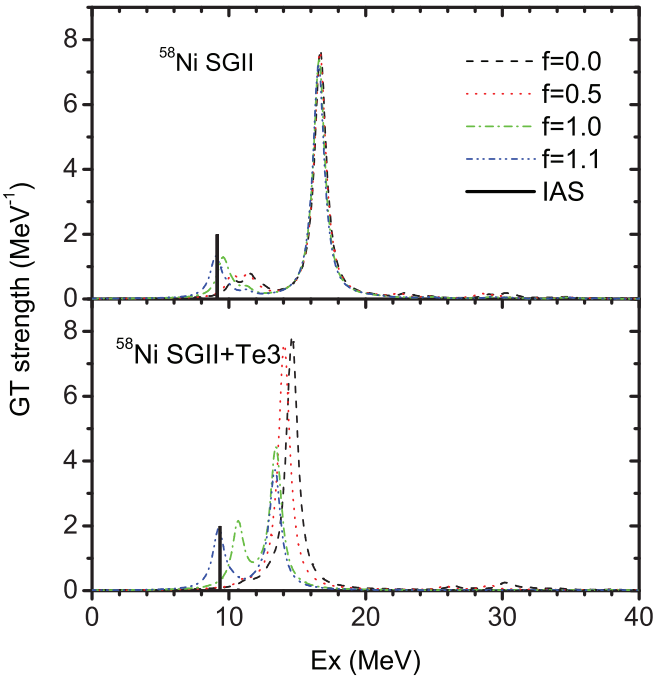

FIG. 15. (Color online) The same as Fig. 3, in the case of ^{58}Ni.

GT strength around the IAR peak is slightly changed. On the other hand, with the tensor correlations included, the main GT peak is shifted downward by more than 2 MeV; moreover, in this case a substantial amount of GT strength is shifted to the lower energy peak in the case of strong isoscalar pairing. The transition amplitudes and their cumulative sum for the low-energy collective states are shown in Fig. 16. The nucleus ^{58}Ni involves many pf-shell configurations, even more than ^{54}Fe, and many unperturbed transitions contribute to the GT strength. For ^{58}Ni, the amplitudes of two states are compared in the upper panel of Fig. 16, namely those of the state at 11.16 MeV (in the case of no isoscalar pairing, $f = 0.0$) and those of the state at 9.25 MeV (in the case of strong isoscalar pairing, $f = 1.1$). With no isoscalar pairing the configuration $(\pi p_{3/2}, \nu p_{3/2})$ at $E_{\rm unp} = 8.0$ MeV is the dominant configuration, while in the case of strong isoscalar pairing ($f = 1.1$), almost all f- and p-shell configurations make important contributions, i.e., $(\pi f_{7/2}, \nu f_{7/2})$, $(\pi f_{5/2}, \nu f_{5/2})$, $(\pi f_{7/2}, \nu f_{5/2})$, $(\pi f_{5/2}, \nu f_{7/2})$, $(\pi p_{3/2}, \nu p_{3/2})$, and $(\pi p_{3/2}, \nu p_{1/2})$. Most of these configurations have the same phase and the GT strength is substantially enhanced by the isoscalar pairing correlations as can be seen in the lower panel of Fig. 16.

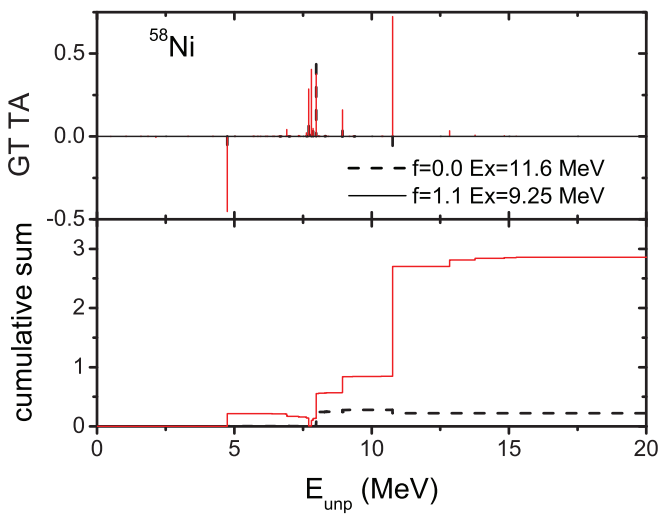

FIG. 16. (Color online) The same as Fig.4 in the case of ^{58}Ni.

F. Characteristic features of the GT distributions in the five nuclei

In ^{42}Ca, the results with the strong isoscalar pairing $f \approx 1.0$ account well for the observed low-energy GT strength below 4 MeV, while those with no or weak isoscalar pairing fail to reproduce the experimental data. For the high-energy region above 4 MeV, the present calculations with the strong IS pairing, $f = 1.0$ or 1.1, can reproduce the strength distribution of ^{42}Ca, but for the heavier nuclei the calculations show a strong concentration of the strength which is different from the experimental data. In addition, the calculations with SGII + Te3 produce a notably higher portion of strength distributed in the low-energy region which means that the tensor force, rather than just the isoscalar pairing force, can affect the ratio of the strengths in the low- and high-energy regions. Namely, the cooperative effect of isoscalar pairing and tensor interaction is noticeable in the low-energy strength in the nuclei at the middle of the pf-shell such as ^{50}Cr, as is shown in Fig. 17. The enhancement of the low-energy strength below 4 MeV is clearly seen in the dash-dotted curve of SGII + Te3 in Fig. 17 in comparison with the dotted curve of SGII without tensor. It is interesting also to notice that SAMi gives an appreciable low-lying strength lying between the two curves of SGII and SGII + Te3.

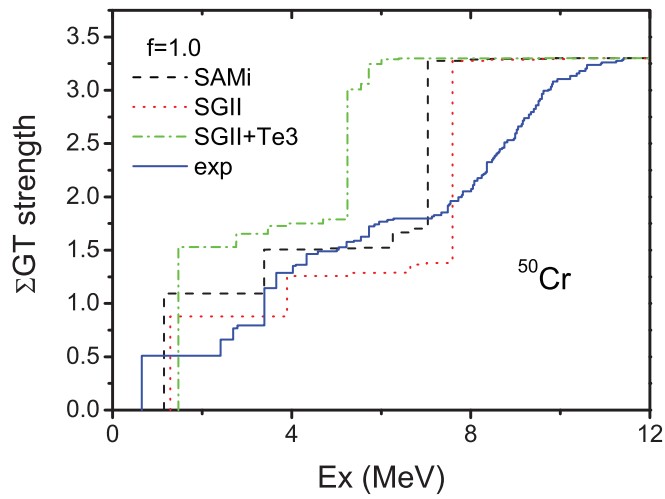

FIG. 17. (Color online) The cumulative sum of the GT strength in ^{50}Cr calculated by SAMi, SGII, and SGII + Te3 interactions with $f = 1.0$. The blue line is the experimental result taken from Refs. [34,39]. The excitation energy is in reference to the IAR. The maximum values of theoretical GT strengths are normalized to that of the experimental result.

There is some fragmentation of the strength in the high-energy region which is still an open question for our present spherical two-quasiparticle QRPA calculation. In general, as we already stressed, we do not aim at reproducing the details of the line shape for the strength distribution. It should be noted that ^{50}Cr and ^{54}Fe are likely to be deformed. The deformation effects on the GT strength have been studied for several $N = Z$ nuclei in the $28 < Z < 50$ region [40], and also in the case of the $N = Z + 2$ nuclei ^{74}Kr, ^{54}Fe, and ^{58}Ni [41,42] (cf. also [43] and references therein). It was shown that deformations (especially oblate) may cause an obvious fragmentation, for instance in the high-energy region of ^{74}Kr, as compared with the spherical case [41]. At the same time, it was shown in Ref. [42] that there is no fragmentation in ^{54}Fe and ^{58}Ni caused by deformation. We should also remind that the coupling with 2p-2h or four-quasiparticle states [44,45], or the particle-vibration coupling (cf. [46,47] and references therein), are not only effective to produce the GT resonance spreading width but at the same time induce strength fragmentation, that increases with increasing excitation energy.

V. CONSTRAINT FOR THE ISOSCALAR PAIRING STRENGTH

The energy differences between the lowest GT and IAR states in $N = Z + 2$ nuclei with mass number $A = 42$–58 obtained by HFB + QRPA calculations are shown in Fig. 18, and compared with the experimental measurements from Refs. [34,39]. The Skyrme parameters SGII, SGII + Te3, and SAMi are used, and systematic calculations are done by varying the $T = 0$ pairing interaction strength, that is, by using $f = 0.0$, 0.5, 0.9, 1.05, and 1.1 [cf. Eq. (2)]. In panel (a), the results of SGII are shown, in which the results of ^{42}Ca, ^{46}Ti, and ^{50}Cr suggest the optimum value of 1.05 for f. For ^{54}Fe and ^{58}Ni, due to the fact that the isovector pairing is somewhat weak (see Fig. 1) and the effect of isoscalar pairing does not manifest itself strongly, the results obtained with $f = 0.9$, 1.0, and 1.05 are quite close and are all acceptable in comparison with the experimental data. In panel (b), SGII + Te3 is used (that is, the tensor force is included) and the mean pairing gap in Fig. 1 is more reasonable as compared with the empirical findings. As a consequence, the effects of isoscalar pairing are more evident, and the results indicate that $f = 1.05$ reproduces well the empirical energy differences between GT and IAR. The interaction SAMi also reproduces reasonably the empirical pairing gaps for the five nuclei in Fig. 1. As shown in panel (c), the GT and IAR energy differences indicate the optimal value of $f = 1.0$–1.05. For all three interactions SGII, SGII + Te3, and SAMi, the optimal isoscalar pairing strength is almost the same with $f = 1.0$–1.05 multiplied by the isovector paring strength for each Skyrme interaction. Thus, we can conclude that the $T = 0$ pairing strength is determined rather uniquely in the study of energy differences between IAS and GT states in the nuclei with $N = Z + 2$.

VI. SUMMARY

HFB + QRPA calculations with the Skyrme forces SGII, SGII + Te3, and SAMi have been performed to study the low-energy GT states in several $N = Z + 2$ nuclei with $A = 42$–58. The isoscalar pairing interaction is taken into account in the QRPA calculations and is shown to have an important effect on the collective low-energy excited GT states in these nuclei.

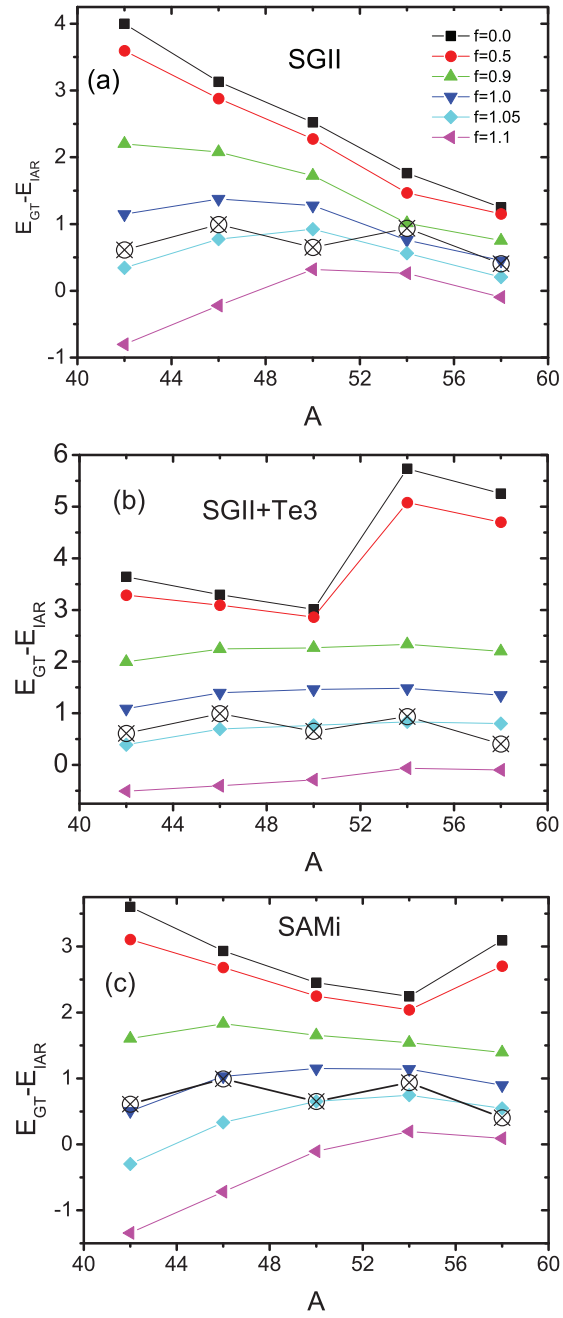

FIG. 18. (Color online) The energy differences between the lowest GT and IAR states in $N = Z + 2$ nuclei with mass number $A = 42$–58 obtained by HFB + QRPA calculations are shown. The interactions SGII + Te3 (with tensor force) and SAMi (without tensor force) are used, and more systematic calculations are done by changing the $T = 0$ pairing interaction, i.e., adopting different values for coupling constant $f = 0.0$, 0.5, 0.9, 0.95, 1.05, and 1.1 [cf. Eq. (2)]. The empty circles with crosses are the experimental data taken from Refs. [34,39].

Without the isoscalar pairing correlations, the low excited GT states are dominated by the $(\nu j_> \rightarrow \pi j_>)$ configurations. When the strong isoscalar pairing interaction $f \approx 1.0$ in Eq. (2) is introduced, the $(\nu j_> \rightarrow \pi j_<)$ configurations are largely mixed with the $(\nu j_> \rightarrow \pi j_>)$ configurations and enhance the GT strength at least several times more than in the case without the isoscalar pairing. In addition to this important effect on the GT strength, the low excited GT states are shifted downward in energy.

This effect is not decoupled, however, from that of the tensor force. We have examined the role of the tensor force by comparing the results of SGII and SGII + Te3. In ^{42}Ca and ^{46}Ti, the effect of the tensor force is invisible in the low-energy peaks, while the high-energy peaks are shifted downward in energy by 1–2 MeV. In the middle of the pf-shell, the low-energy peaks are also affected significantly by the tensor force, both in energy and in strength, in ^{50}Cr, ^{54}Fe, and ^{58}Ni. This difference is mainly due to the presence of several configurations excited from both f- and p-orbits in the GT states of the heavier pf-shell nuclei.

To highlight these points, in our paper we have carried out systematic calculations, with different strengths of the isoscalar pairing, and compared our results with the empirical energy difference between the low excited collective GT and IAR states of five nuclei with $N = Z + 2$. Our main result is that the optimal strength of the isoscalar pairing is obtained to be 1.0 to 1.05 times the isovector pairing strength, independent on the adopted Skyrme interaction. In other words, the isoscalar pairing strength is determined unambiguously in the present study of the low energy GT strength.

The global GT strength distribution has also been discussed by means of the cumulative GT sum plots. For ^{42}Ca, the cumulative sum of the experimentally observed GT strengths is qualitatively and quantitatively well reproduced by the present calculations with the strong isoscalar pairing $f \approx 1.0$. In ^{46}Ti, ^{50}Cr, ^{54}Fe, and ^{58}Ni, the present QRPA calculation can reproduce the position and the portion of strength of the GT states in the low-energy region (i.e., within 4 MeV above the IAR). In the higher energy region, the empirical GT strength is fragmented in many bump-like states; the QRPA calculations show that the GT strengths are concentrated in one main state. This is probably not surprising as we miss spreading effects that go beyond the simple QRPA.

Finally, it is confirmed from the present study that the excitation energies and strengths of the low energy GT states in $N \sim Z$ nuclei could be one of the most promising candidates to disentangle the isoscalar pairing correlations and constrain the corresponding strength.

ACKNOWLEDGMENTS

This work is supported by the National Natural Science Foundation of China under Grants No. 11105094 and No. 11375266, and Outstanding Young Scholar research fund of Sichuan University, Grant No. 2082604174215. This work was also supported by the Japanese Ministry of Education, Culture, Sports, Science and Technology by a Grant-in-Aid for Scientific Research under the program number (C) 22540262.

[1] A. Bohr, B. R. Mottelson, and D. Pines, Phys. Rev. **110**, 936 (1958).
[2] A. Bohr and B. R. Mottelson, *Nuclear Structure*, Vol. I (Benjamin, New York, 1969).
[3] D. M. Brink and R. Broglia, *Nuclear Superfluidity: Pairing in Finite Systems* (Cambridge University Press, Cambridge, UK, 2005).
[4] D. Vautherin, Phys. Rev. C **7**, 296 (1973).
[5] J. Dobaczewski, H. Flocard, and J. Treiner, Nucl. Phys. A **422**, 103 (1984).
[6] M. Bender, P.-H. Heenen, and P.-G. Reinhard, Rev. Mod. Phys. **75**, 121 (2003).
[7] M. V. Stoitsov, J. Dobaczewski, W. Nazarewicz, and P. Borycki, Int. J. Mass Spectrom. **251**, 243 (2006).
[8] T. Duguet, P. Bonche, P.-H. Heenen, and J. Meyer, Phys. Rev. C **65**, 014311 (2001).
[9] J. Margueron, H. Sagawa, and K. Hagino, Phys. Rev. C **76**, 064316 (2007); **77**, 054309 (2008).
[10] D. J. Rowe, *Nuclear Collective Motion* (Methuen, London, 1970).
[11] J. Terasaki, J. Engel, M. Bender, J. Dobaczewski, W. Nazarewicz, and M. Stoitsov, Phys. Rev. C **71**, 034310 (2005).
[12] J. Engel, M. Bender, J. Dobaczewski, W. Nazarewicz, and R. Surman, Phys. Rev. C **60**, 014302 (1999).
[13] M. Matsuo, Nucl. Phys. A **696**, 371 (2001).
[14] E. Khan, N. Sandulescu, M. Grasso, and Nguyen Van Giai, Phys. Rev. C **66**, 024309 (2002).
[15] N. Paar, P. Ring, T. Nikšić, and D. Vretenar, Phys. Rev. C **67**, 034312 (2003).
[16] A. L. Goodman, Nucl. Phys. A **186**, 475 (1972).
[17] A. L. Goodman, Phys. Rev. C **60**, 014311 (1999).
[18] A. Poves and G. M. Pinedo, Phys. Lett. B **430**, 203 (1988).
[19] E. Garrido, P. Sarriguren, E. Moya de Guerra, and P. Schuck, Phys. Rev. C **60**, 064312 (1999).
[20] E. Garrido, P. Sarriguren, E. Moya de Guerra, U. Lombardo, P. Schuck, and H. J. Schulze, Phys. Rev. C **63**, 037304 (2001).
[21] G. F. Bertsch and Y. Luo, Phys. Rev. C **81**, 064320 (2010).
[22] A. Gezerlis, G. F. Bertsch, and Y. L. Luo, Phys. Rev. Lett. **106**, 252502 (2011).
[23] I. N. Borzov and S. Goriely, Phys. Rev. C **62**, 035501 (2000).
[24] K. Yoshida, Prog. Theor. Exp. Phys. (2013) 113D02.
[25] J. Suhonen and O. Civitarese, Phys. Rep. **300**, 123 (1998).
[26] S. Fracasso and G. Colò, Phys. Rev. C **76**, 044307 (2007).
[27] N. V. Giai and H. Sagawa, Phys. Lett. B **106**, 379 (1981).
[28] M. Bender, J. Dobaczewski, J. Engel, and W. Nazarewicz, Phys. Rev. C **65**, 054322 (2002).
[29] C. L. Bai, H. Sagawa, H. Q. Zhang, X. Z. Zhang, G. Colò, and F. R. Xu, Phys. Lett. B **675**, 28 (2009).
[30] C. L. Bai, H. Q. Zhang, X. Z. Zhang, F. R. Xu, H. Sagawa, and G. Colò, Phys. Rev. C **79**, 041301(R) (2009).

[31] F. Minato and C. L. Bai, Phys. Rev. Lett. **110**, 122501 (2013).
[32] M. Sasano *et al.*, Phys. Rev. Lett. **107**, 202501 (2011).
[33] C. L. Bai, H. Sagawa, M. Sasano, T. Uesaka, K. Hagino, H. Q. Zhang, X. Z. Zhang, and F. R. Xu, Phys. Lett. B **719**, 116 (2013).
[34] Y. Fujita *et al.*, Phys. Rev. Lett. **112**, 112502 (2014).
[35] Y. Tanimura, H. Sagawa, and K. Hagino, Prog. Theor. Exp. Phys. (2014) 053D02.
[36] C. L. Bai, H. Q. Zhang, H. Sagawa, X. Z. Zhang, G. Colò, and F. R. Xu, Phys. Rev. C **83**, 054316 (2011).
[37] X. Roca-Maza, G. Colò, and H. Sagawa, Phys. Rev. C **86**, 031306(R) (2012).
[38] G. F. Bertsch and S. E. Tsai, Phys. Rep. **18**, 127 (1975).
[39] H. Fujita *et al.*, Phys. Rev. C **75**, 034310 (2007).
[40] F. Frisk, I. Hamamoto, and X. Z. Zhang, Phys. Rev. C **52**, 2468 (1995).
[41] P. Sarriguren, E. Moya de Guerra, A. Escuderos, and A. C. Carrizo, Nucl. Phys. A **635**, 55 (1998).
[42] P. Sarriguren, E. Moya de Guerra, and R. Álvarez-Rodríguez, Nucl. Phys. A **716**, 230 (2003).
[43] P. Sarriguren, Phys. Rev. C **87**, 045801 (2013).
[44] A. Arima, K. Shimizu, W. Bentz, and H. Hyuga, Adv. Nucl. Phys. **18**, 1 (1988).
[45] G. F. Bertsch and I. Hamamoto, Phys. Rev. C **26**, 1323 (1982).
[46] Y. F. Niu, G. Colò, M. Brenna, P. F. Bortignon, and J. Meng, Phys. Rev. C **85**, 034314 (2012).
[47] Y. F. Niu, G. Colò, and E. Vigezzi (unpublished).